Supporting Information

Remote Plasma Polymers of Iron (II) Phthalocyanine in Polyacrylonitrile-Derived Carbon Electrospun Fibres as Electrode for Supercapacitors.

Jose M. Obrero [a*], Jorge PV Tafoya [b], Michael Thielke [b], G.P. Moreno-Martínez [a], Lidia Contreras-Bernal [a,c], Jose Ferreira de Sousa Jr [a], Juan Ramón Sánchez-Valencia [a], Angel Barranco [a], and Ana B. Jorge Sobrido [b*].

a) Nanotechnology on Surfaces and Plasma Laboratory, Materials Science Institute of Seville (CSIC-US), C/ Américo Vespucio 49, 41092, Seville, Spain.

b) Centre for Sustainable Engineering, School of Engineering and Materials Science, Faculty of Science and Engineering, Queen Mary University of London, Mile End Road, London, E1 4NS, UK

c) Química-Física. Department of Physical Chemistry, University of Seville, C/Professor García González n° 2, Seville 41012, Spain

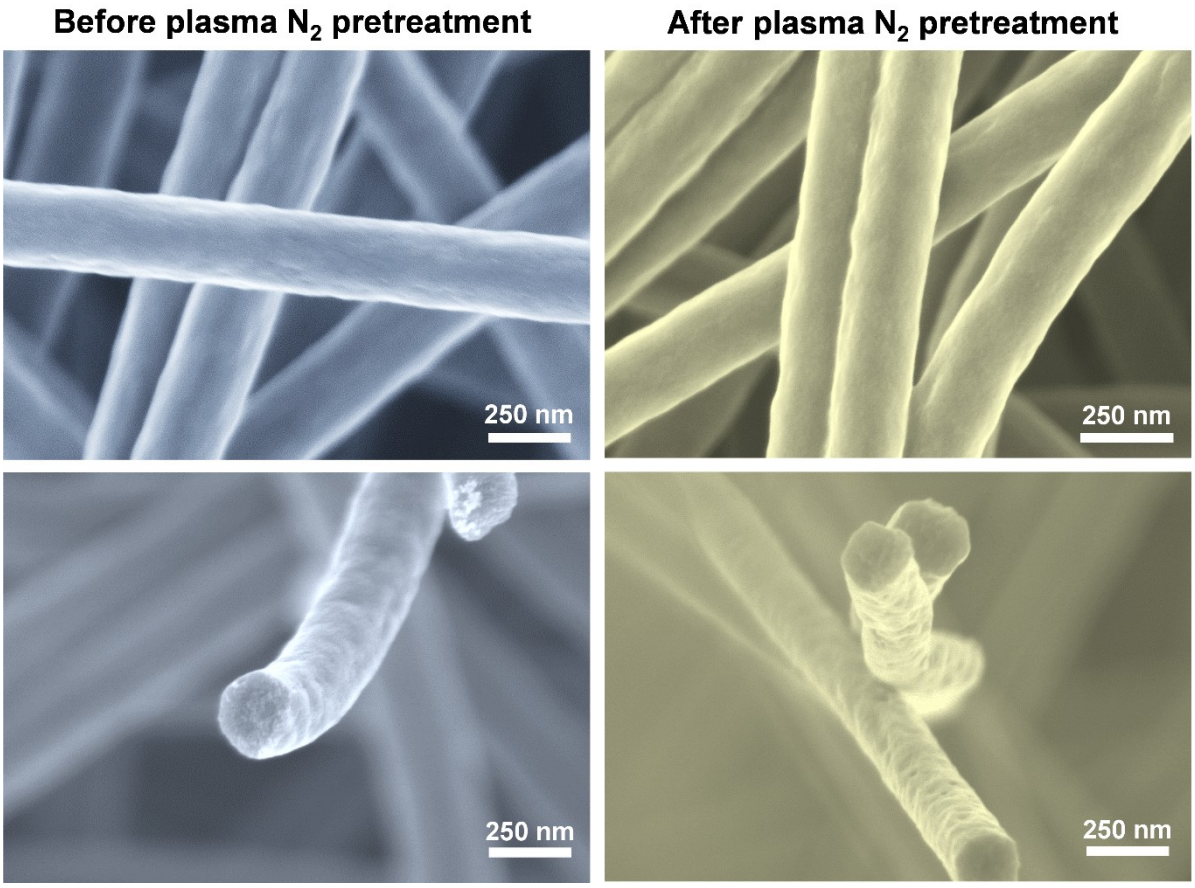

Figure S1. Comparative SEM micrographs of carbon nanofibres (CNFs) before and after N_2 plasma treatment. The untreated CNFs exhibit smooth and clean surfaces, characteristic of electrospun and carbonized PAN fibres. After exposure to N_2 plasma, the overall morphology and fibre diameter remain unchanged, confirming that the process is mild and does not cause structural damage. However, a slight increase in surface roughness can be observed, indicating the introduction of surface defects and nitrogen-containing functional groups that enhance the surface reactivity and adhesion for subsequent FePc deposition.

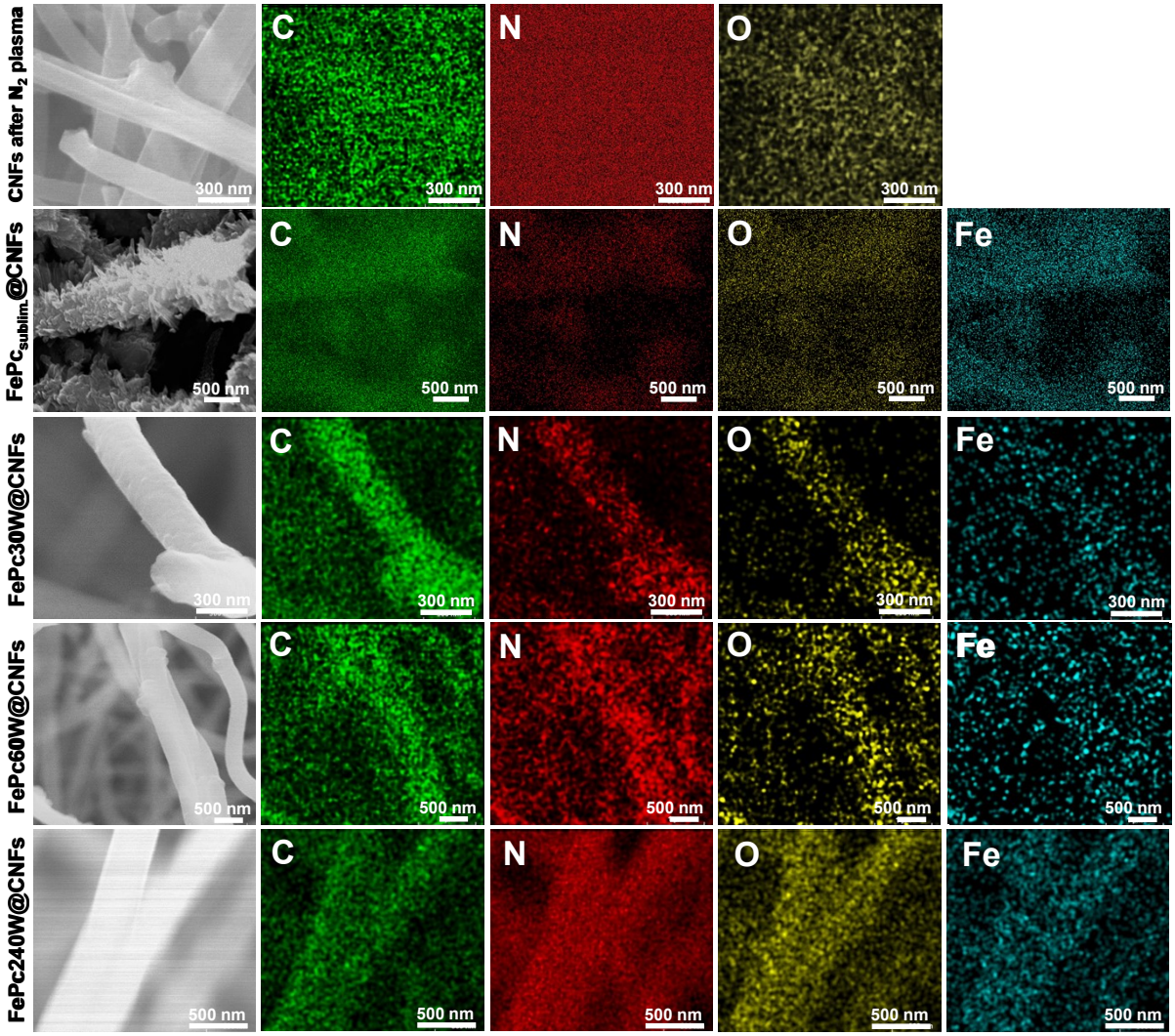

Figure S2. EDX elemental mapping of CNFs after N_2 plasma pretreatment, sublimated FePc and RPAVD-N_2 FePc coatings deposited at different plasma powers. Elemental distributions of C (green), N (red), O (yellow) and Fe (blue).

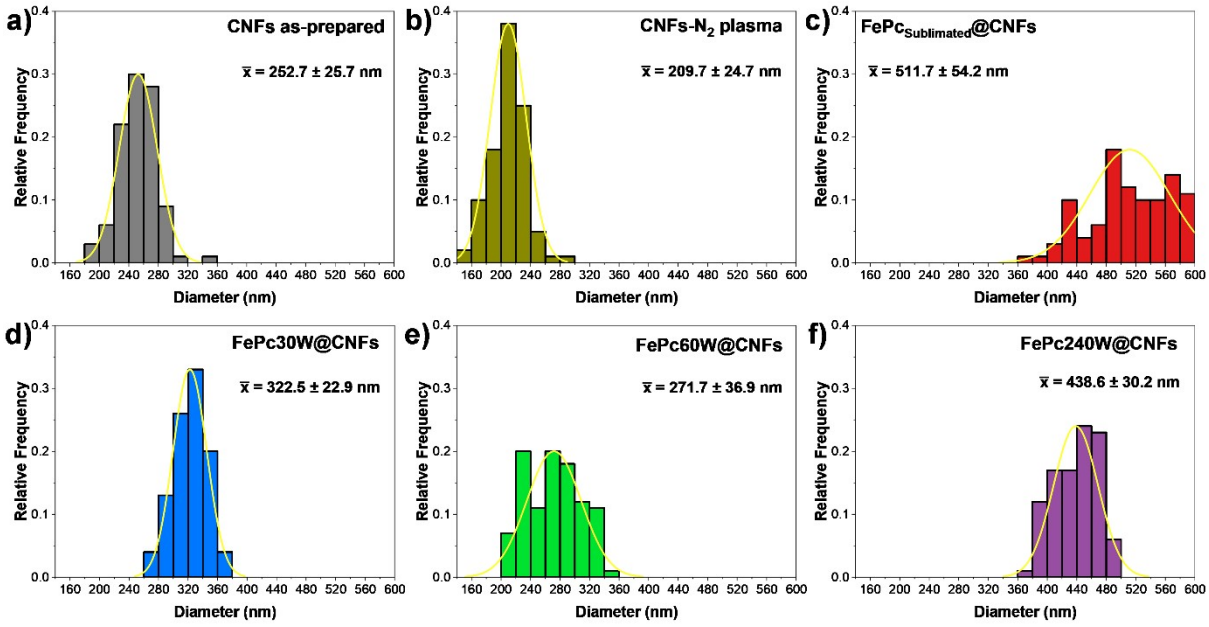

Figure S3. Diameter size distribution of CNFs samples determined from the analysis of SEM micrographs of a) CNFs as-prepared, b) CNFs after N_2 plasma treatment, c) $FePc_{Sublimated}$@CNFs, d) FePc30W@CNFs, e) FePc60W@CNFs and f) FePc240W@CNFs.

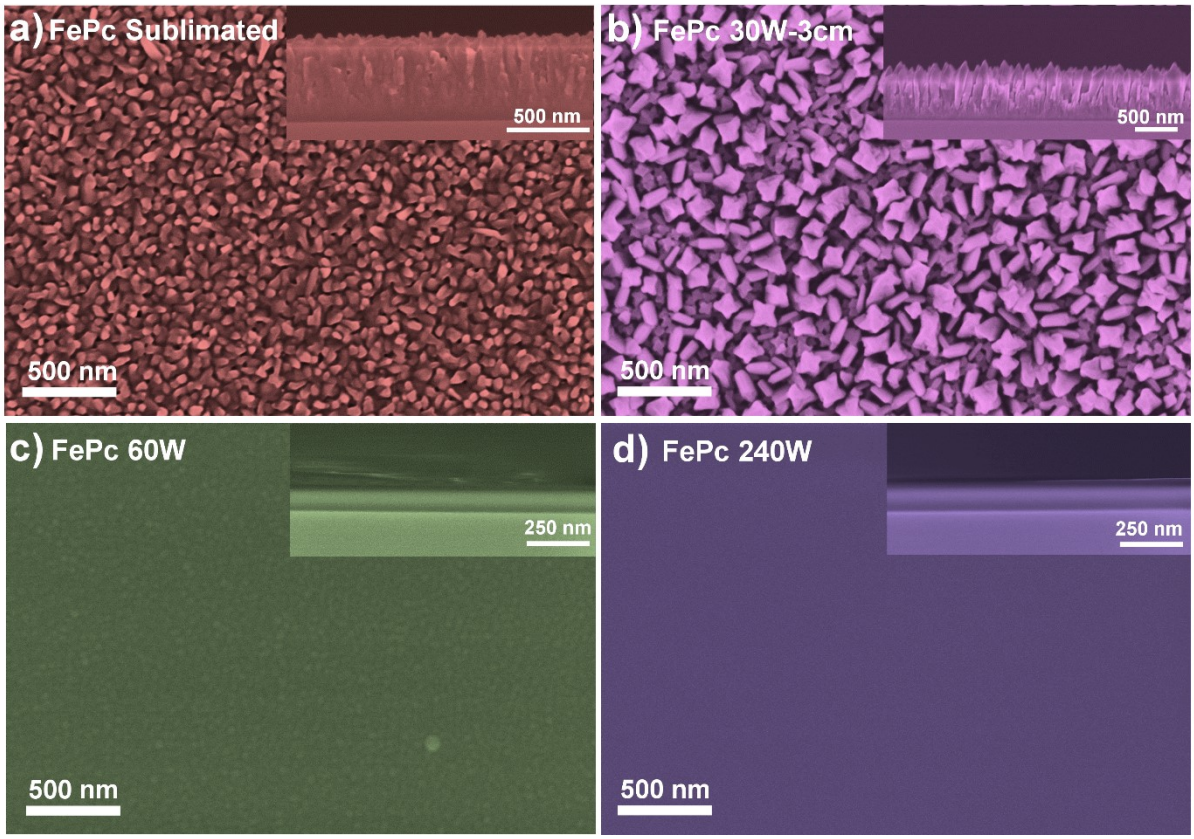

Figure S4. Top-view SEM micrographs and cross-sectional (inset) SEM images of FePc films on silicon: sublimated FePc and FePc plasma polymers deposited by RPAVD-N_2 at different polymerization degrees. (a) Sublimated FePc; (b) 30 W–3 cm; (c) 60 W; and (d) 240 W.

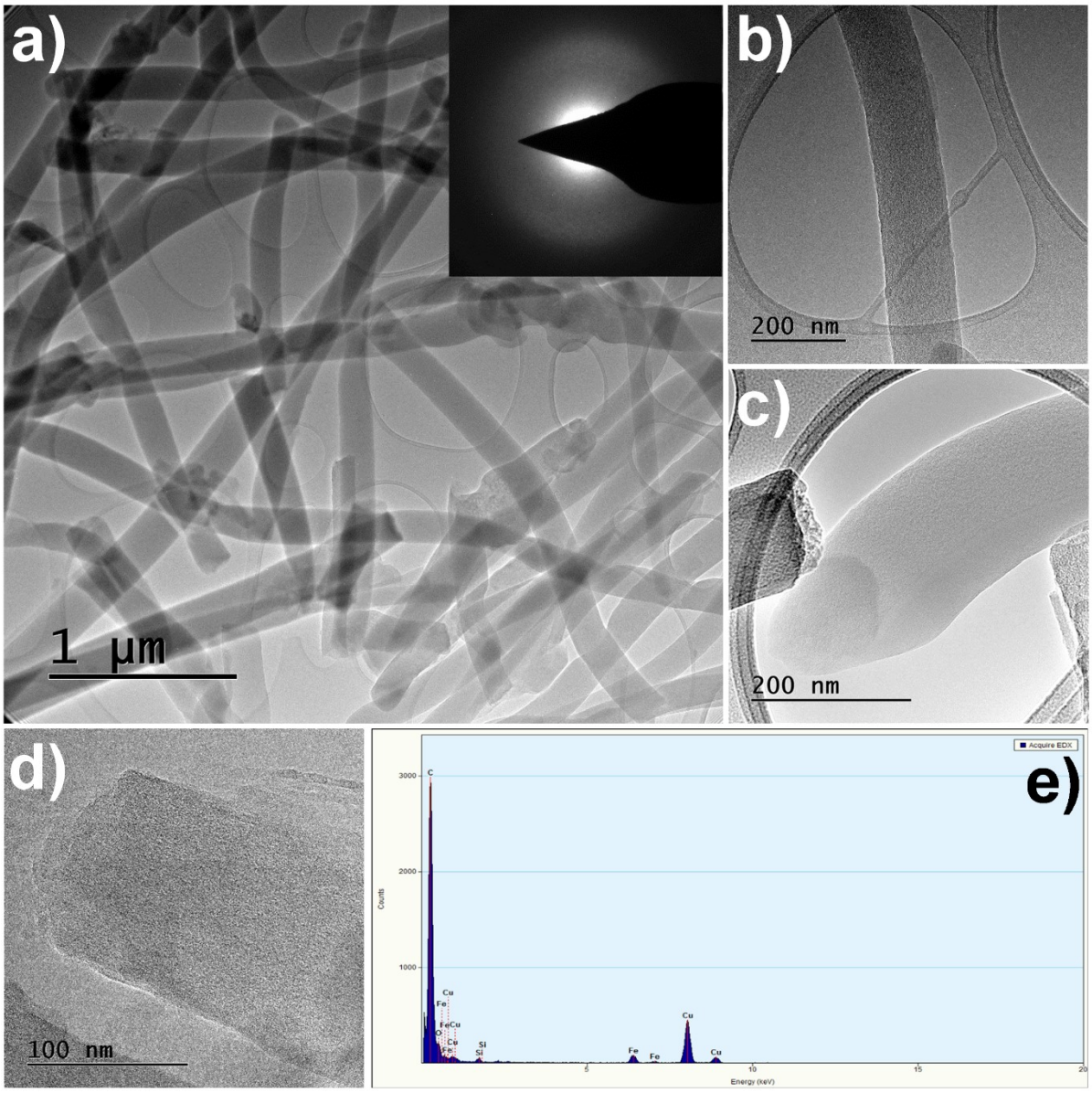

Figure S5. (a-d) TEM micrographs of a FePc60W@CNFs sample showing carbon nanofibres uniformly coated with the plasma-polymerised FePc layer. A continuous shell is clearly observed around each fibre. The inset in (a) shows the SAED pattern displaying a diffuse halo, confirming the amorphous nature of the plasma-polymerised coating. **(e)** STEM-EDX elemental mapping of the sample.

Table S1. Areal mass loading of the FePc plasma-polymer thin films determined by Rutherford Backscattering Spectrometry (RBS). The measurements correspond exclusively to the plasma-polymer coating deposited under each RPAVD-N_2 condition.

Sample	Mass loading ($mg \cdot cm^{-2}$)
FePc30W_3cm	0.063
FePc30W	0.024
FePc60W	0.017
FePc240W	0.021

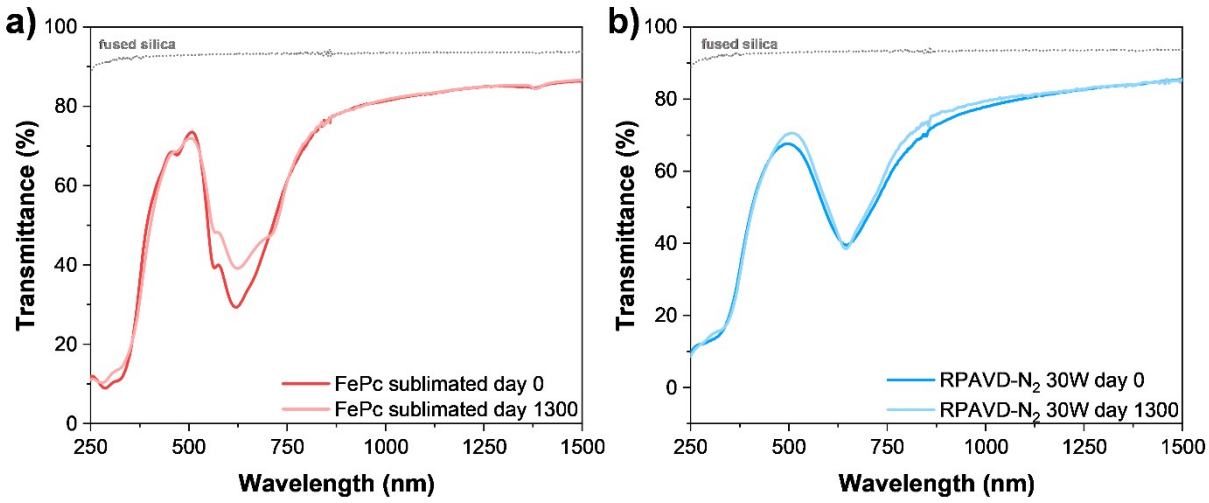

Figure S6. UV–Vis–NIR transmittance spectra of (a) sublimated FePc and (b) FePc30 W thin films, comparing as-deposited samples with those after air-exposure degradation for 1300 days.

The survey spectra and the atomic percentages of each element are shown in **Figures S7a and S7c**, respectively. Notable differences were observed in the relative amounts of carbon, nitrogen, and oxygen before and after N_2 plasma exposure. Specifically, the as-prepared CNFs contain C = 85.7%, N = 9.2%, O = 4.8%, and Na = 0.3%; whereas the plasma-treated CNFs exhibit C = 69.5%, N = 18.0%, O = 10.4%, and Na = 2.0%. These results confirm the incorporation of nitrogen-containing functional groups from the plasma into the fibrous matrix. The presence of sodium is most likely due to contamination introduced during handling, stabilisation or carbonisation.

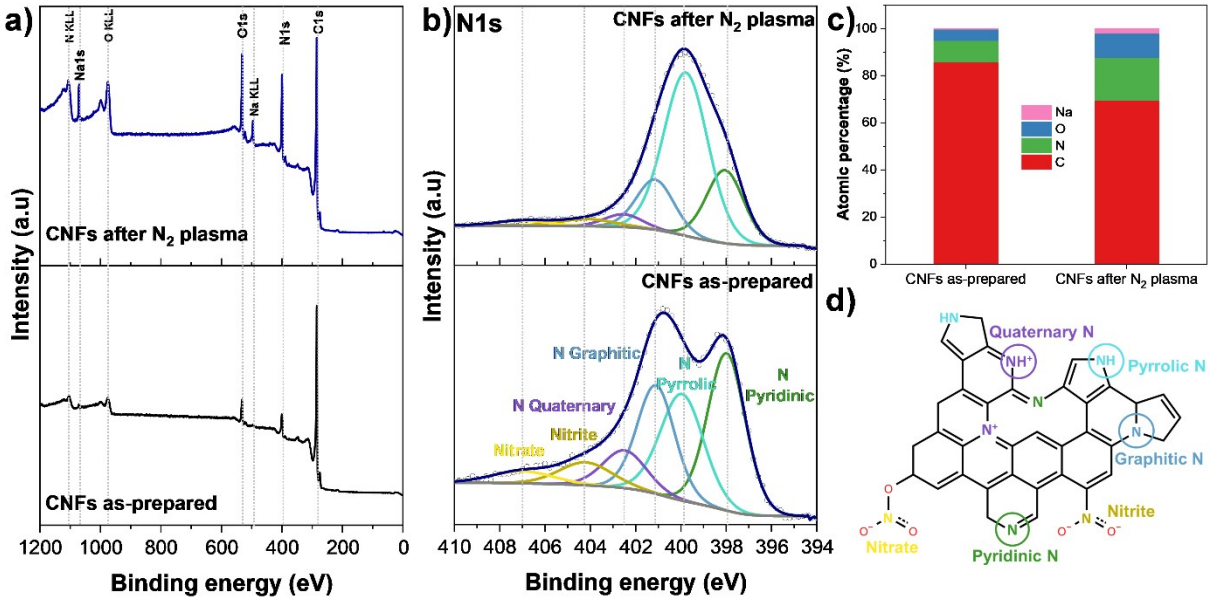

Figure S7. (a) XPS survey spectra of CNFs before and after N_2 plasma pretreatment. (b) High-resolution N1s spectra highlighting the evolution of nitrogen species upon plasma exposure. (c) Atomic percentages of C, N, O, and Na quantified from the XPS data. Both samples display the characteristic features of nitrogen-doped carbon materials, including pyridinic N (398.0 eV), pyrrolic N (399.9 eV), graphitic N (401.1 eV), and positively charged quaternary N (402.5 eV), as well as oxidized nitrogen species, namely $–NO_2$ (404.2 eV) and $–NO_3$ (407.0 eV).[1] After N_2 plasma treatment, the pyrrolic-N component increases markedly at the expense of the other species, indicating that the plasma induces a soft etching process that partially fragments the carbon rings. The highly reactive N_2 species then react with the resulting carbon radicals, promoting the incorporation of additional nitrogen and the formation of new pyrrolic-type sites. This nitrogen enrichment, particularly in pyrrolic-type sites, is expected to influence the coordination behaviour of FePc upon deposition. (d) Schematic representation of nitrogen functionalities and defect sites introduced into the CNF surface.

(1) Hellgren, N.; Haasch, R. T.; Schmidt, S.; Hultman, L.; Petrov, I. Interpretation of X-Ray Photoelectron Spectra of Carbon-Nitride Thin Films: New Insights from in Situ XPS. *Carbon* **2016**, *108*, 242–252. https://doi.org/10.1016/j.carbon.2016.07.017.

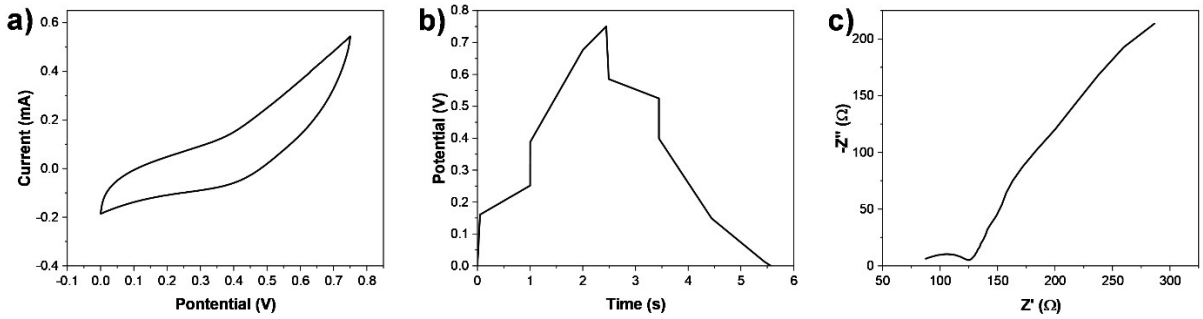

Figure S8. Electrochemical performance of N_2 plasma pre-treated CNTs. (a) Cyclic voltammetry curve recorded at a scan rate of 10 $mV \cdot s^{-1}$. (b) Galvanostatic charge-discharge profile measured at a current density of 0.25 $A \cdot g^{-1}$. (c) Electrochemical impedance spectroscopy (EIS) response.

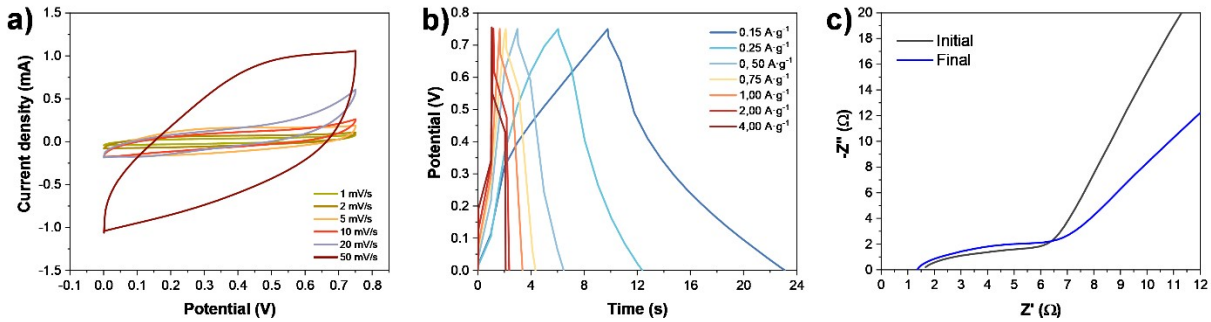

Figure S9. Electrochemical performance of $FePc_{sublimated}$@CNFs electrode. (a) Cyclic voltammetry curve recorded at a scan rate of 10 $mV \cdot s^{-1}$. (b) Galvanostatic charge-discharge profile measured at a current density of 0.25 $A \cdot g^{-1}$. (c) Electrochemical impedance spectroscopy (EIS) response.

Table S2. Coefficients of the pseudocapacitive model $i(v)=k_1 \cdot v+k_2 \cdot v^{1/2}$ at selected voltages.

Potential	k_1 ($mA \cdot mV^{-1} \cdot s^{-2}$)	Error k_1	k_2 ($mA \cdot mV^{-1} \cdot s^{-1/2}$)	Error k_2	R^2
0.00 V	-0.069850	±0.010320	-0.161090	±0.060580	0.99072
0.40 V (forward)	0.079900	±0.008600	0.152616	±0.050600	0.99480
0.75 V	0.077922	±0.006861	0.213459	±0.040260	0.99697
0.40 V (reverse)	-0.075000	±0.009700	-0.139800	±0.056700	0.99250

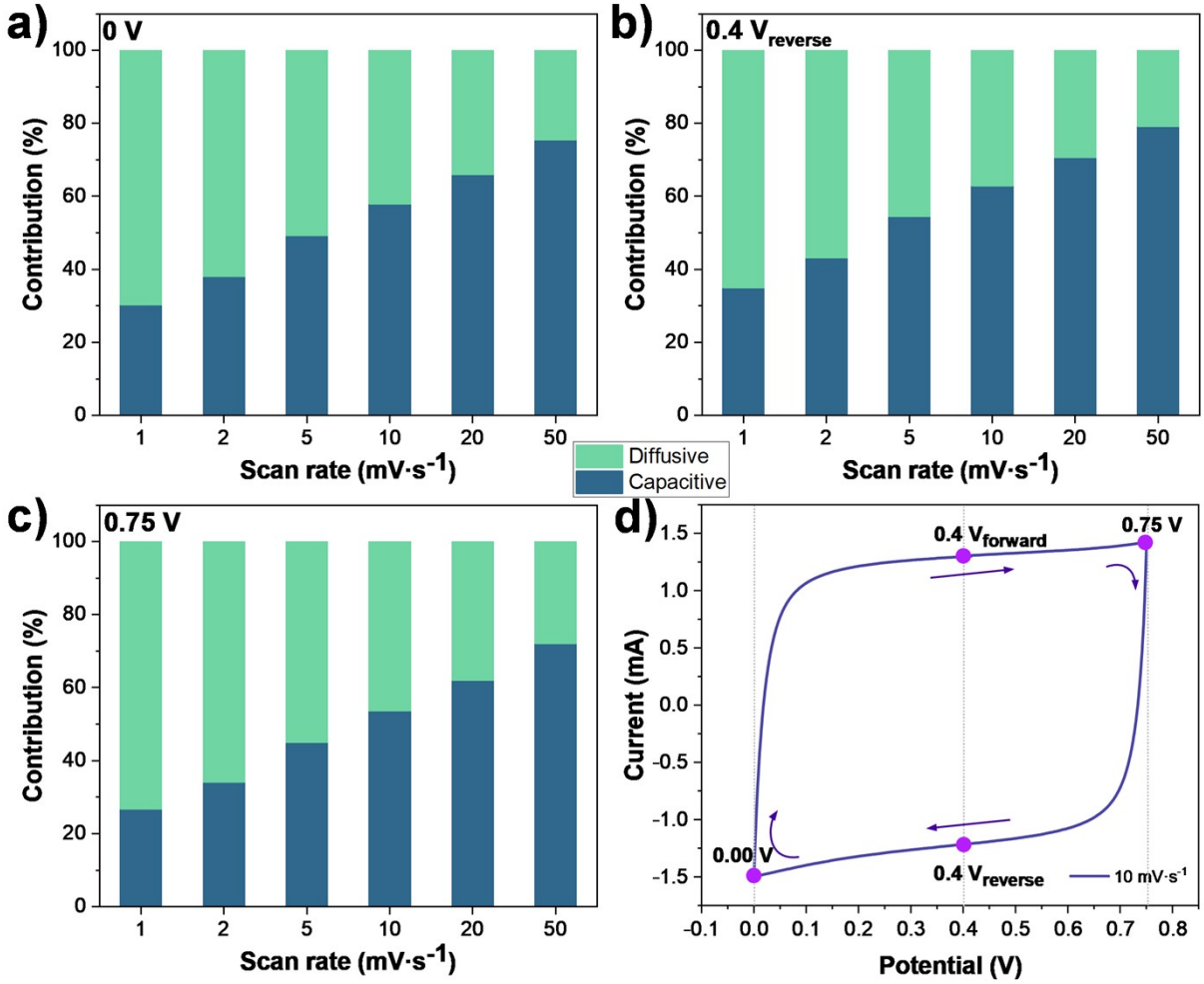

Figure S10. Deconvolution of capacitive and diffusive contributions at selected potentials for FePc30W@CNFs electrodes. Bar graphs showing the relative contributions of capacitive (blue) and diffusive (green) currents at scan rates from 1 to 50 $mV \cdot s^{-1}$, extracted at: (a) 0.00 V, (b) 0.40 V (reverse scan) and (c) 0.75 V. Cyclic voltammogram highlighting the selected potentials (magenta dots) used for the deconvolution analysis.

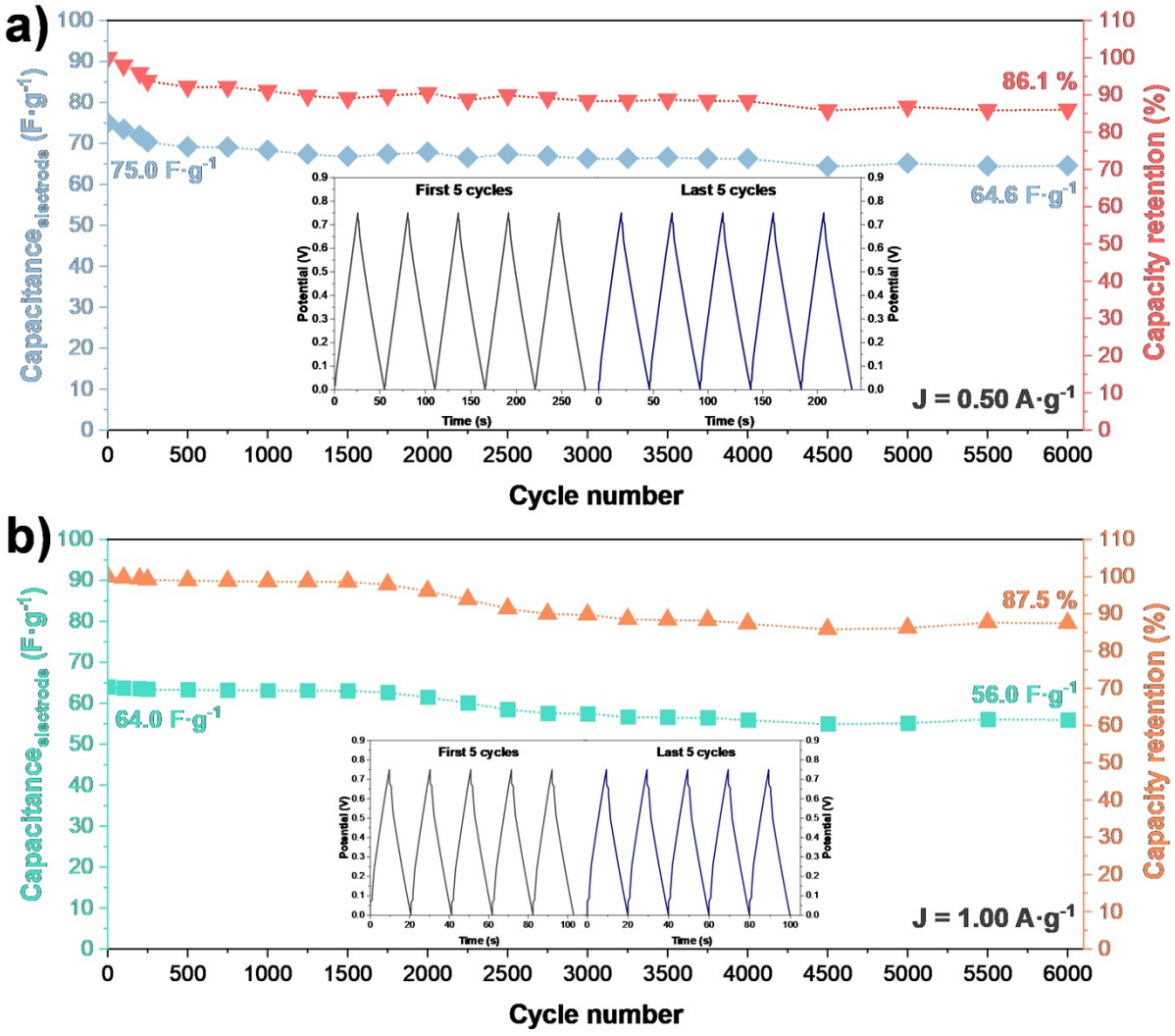

Figure S11. Cycling stability and capacitance retention of FePc30W@CNFs at (a) 0.50 $A \cdot g^{-1}$ and (b) 1.00 $A \cdot g^{-1}$. Each inset shows the first and last five cycles during the stability test.

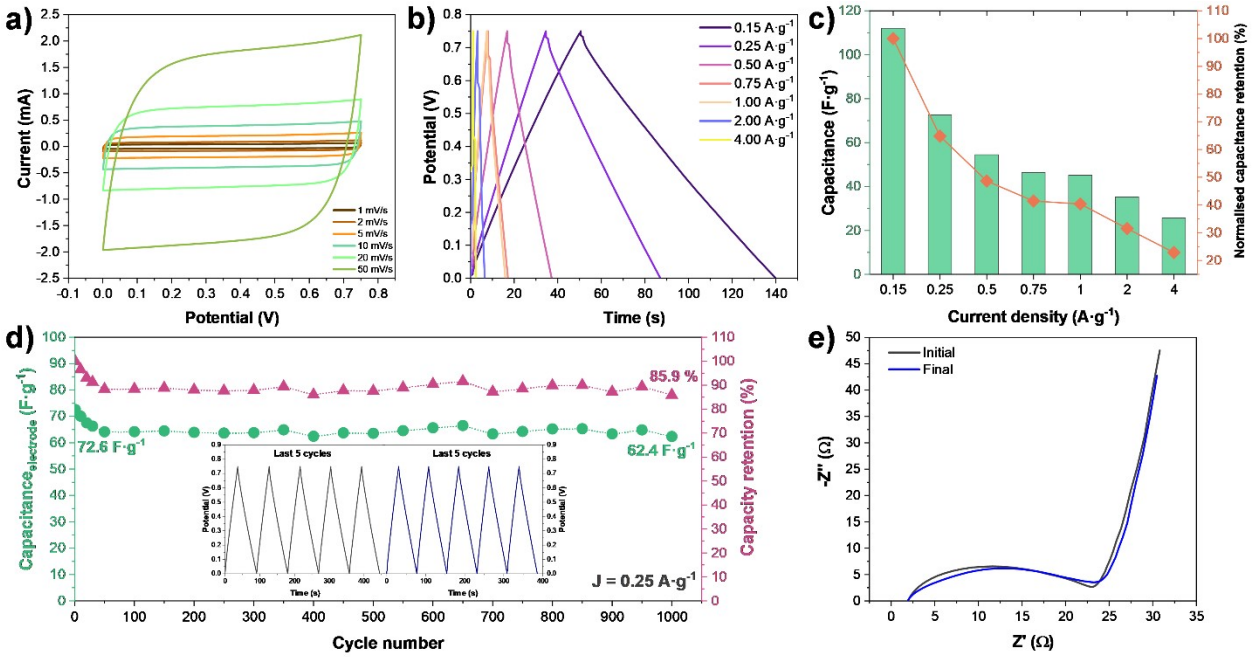

Figure S12. Electrochemical performance of FePc60W@CNFs sample. (a) CV curves recorded at scan rates ranging from 1 to 50 $mV \cdot s^{-1}$. (b) GCD curves recorded at various current densities. (c) Specific capacitance ($C_{electrode}$) as a function of current density, along with the normalised capacitance relative to the lowest current density (0.15 $A \cdot g^{-1}$). (d) Cycling stability and capacitance retention at 0.25 $A \cdot g^{-1}$. The inset shows the first and last five cycles during the stability test. (e) Nyquist plots recorded before and after cycling.

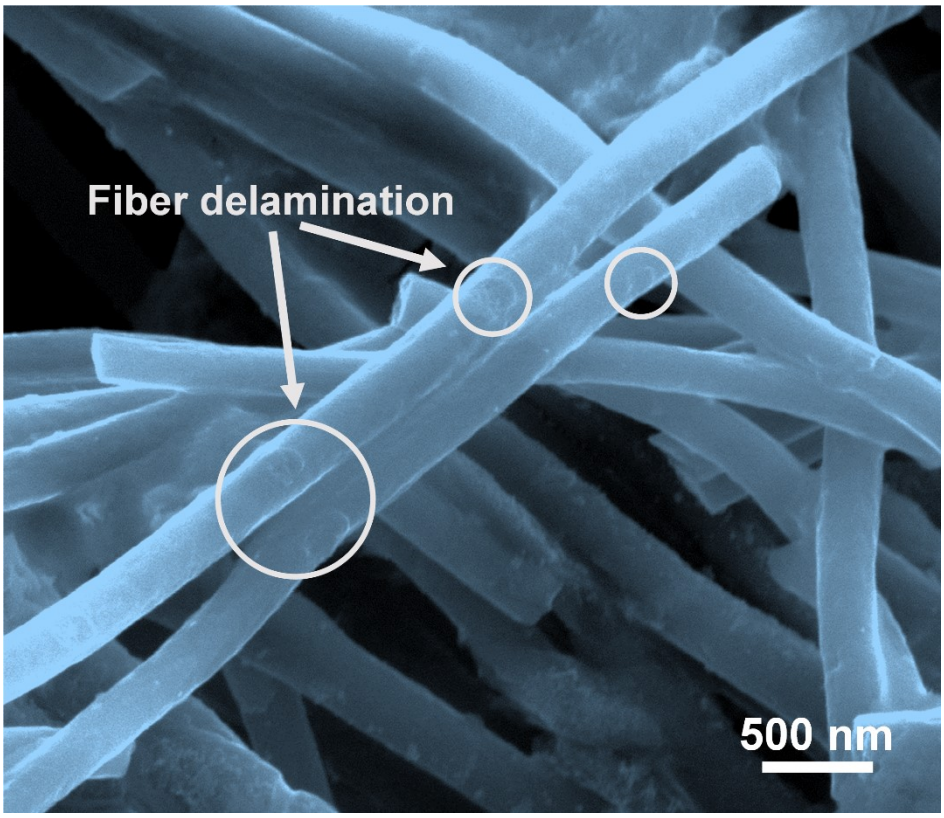

Figure S13. SEM micrographs of post-treated FePc30W@CNFs sample after 6000 charge-discharge cycles. Regions of partial delamination of the plasma-polymer coating have been labelled, attributed to electrode-electrolyte separation during cycling, which leads to the exposure of bare fibre areas.

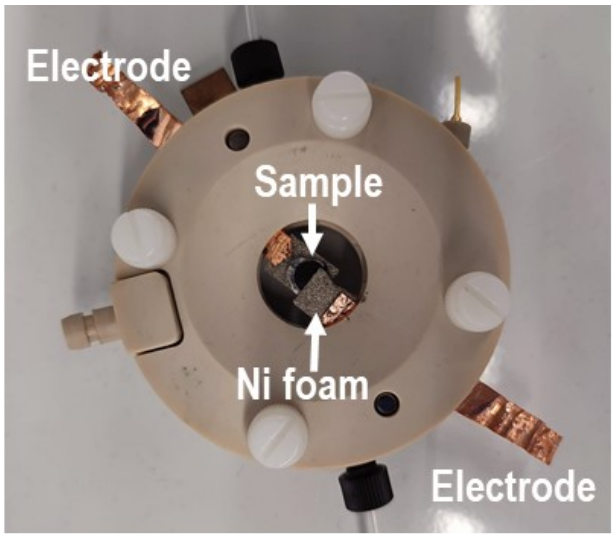

Figure S14. Top-view of the experimental set-up of *in situ* Raman measurements.

Table S3. Comparison of the result of this study with previous similar works on supercapacitor based in metal-phathalocyanines.

Electrode type	Method	Specific Capacitance	Energy Density	Power Density	Cycling stability		Electrolyte	Ref.
					No. of cycles	Capacitance retention (%)		
FePc@C-HTC	Hydrothermal carbonisation + pyrolisis	48 $F \cdot g^{-1}$ at 0.2 $A \cdot g^{-1}$	1.7 $Wh \cdot kg^{-1}$	140.3 $W \cdot kg^{-1}$	10000 at 5 $A \cdot g^{-1}$	99	2M H_2SO_4	[15]
FePc@GO	Self-assembly via π-π interactions	235.5 $F \cdot g^{-1}$ at 1 $A \cdot g^{-1}$	8.2 $Wh \cdot kg^{-1}$	531.9 $W \cdot kg^{-1}$	60000 at 5 $A \cdot g^{-1}$	100	6M KOH	[16]
FePc@NC-1000	MOF synthesis + CVD carbonisation + FePc assembly	0.03 $F \cdot cm^{-2}$ at 5.96 $A \cdot cm^{-2}$	n/a	0.12 $W \cdot cm^{-2}$	10 h duration	98.4	Alcaline solution	[66]
FePc@MWNCTs	one step in-situ precipitation	65.3 $F \cdot g^{-1}$ at 0.25 $A \cdot g^{-1}$	29.7 $Wh \cdot kg^{-1}$	125.0 $W \cdot kg^{-1}$	30000 at 8 $A \cdot g^{-1}$	111.3	1M H_2SO_4	[65]
CoPc@CNTs	acid-treated CNTs + CoPc ultrasonication	1112 $F \cdot g^{-1}$ at 1 $A \cdot g^{-1}$	55.6 $Wh \cdot kg^{-1}$	122.0 $W \cdot kg^{-1}$	1000 at 1 $A \cdot g^{-1}$	95	6M KOH	[14]
nCuPc+TiN	Hydrotermal	29.7 $F \cdot g^{-1}$ at 0.25 $A \cdot g^{-1}$	2.4 $Wh \cdot kg^{-1}$	388 $W \cdot kg^{-1}$	30000 at 0.5 $A \cdot g^{-1}$	93.5	1M Na_2SO_4	[67]
β-ZnPc molecular crystal	Ring-closure reaction+annealing at 400 ºC	49.1 $F \cdot g^{-1}$ at 0.10 $A \cdot g^{-1}$	86.2 $Wh \cdot kg^{-1}$	220 $W \cdot kg^{-1}$	100000 at 2 $A \cdot g^{-1}$	73.4	PVA/$Zn(CF_3SO_3)_2$ gel	[68]
NiPc@MWCNT	MWCNTs + NiPc ultrasonication	0.19 $F \cdot cm^{-2}$ at 1 $mA \cdot cm^{-2}$	0.05 $Wh \cdot cm^{-2}$	0.7 $W \cdot cm^{-2}$	5000 at 10 $mA \cdot cm^{-2}$	60	PBS/KFC	[11]
CoPc@MWCNT	MWCNTs + CoPc ultrasonication	0.51 $F \cdot cm^{-2}$ at 1 $mA \cdot cm^{-2}$	0.14 $Wh \cdot cm^{-2}$	0.7 $W \cdot cm^{-2}$	5000 at 10 $mA \cdot cm^{-2}$	92	PBS/KFC	[11]
NiPc NF-rGO	NiPc nanofibre synthesis + rGO hydrothermal assembly	223.3 $F \cdot g^{-1}$ at 1 $A \cdot g^{-1}$	15.2 $Wh \cdot kg^{-1}$	349.9 $W \cdot kg^{-1}$	1000 at 1 $A \cdot g^{-1}$	n/a	1M H_2SO_4	[69]
NiPc@C-HTC	Hydrothermal carbonisation + pyrolisis	48 $F \cdot g^{-1}$ at 0.2 $A \cdot g^{-1}$	≈1.6 $Wh \cdot kg^{-1}$	≈120 $W \cdot kg^{-1}$	10000 at 5 $A \cdot g^{-1}$	98	2M H_2SO_4	[15]
Plasma polymer of FePc@electrospun CNFs	**Remote plasma N_2 assisted vapour deposition**	**80.9 $F \cdot g^{-1}$ at 0.25 $A \cdot g^{-1}$** and **0.79 $F \cdot cm^{-2}$ at 4.87 $mA \cdot cm^{-2}$**	**6.3 $Wh \cdot kg^{-1}$** and **$6.2 \cdot 10^{-5}$ $Wh \cdot cm^{-2}$**	**375 $W \cdot kg^{-1}$** and **$3.6 \cdot 10^{-4}$ $W \cdot cm^{-2}$**	**6000 at 1 $A \cdot g^{-1}$** and **6000 at 19.4 $mA \cdot cm^{-2}$**	**87.5**	**6M KOH**	**This work**